

Influence of the projectile description on breakup calculations

P. Capel^{1,*} and F. M. Nunes^{2,†}

¹*TRIUMF, 4004 Wesbrook Mall, Vancouver, B.C., Canada V6T2A3*

²*National Superconducting Cyclotron Laboratory and Department of Physics and Astronomy,
Michigan State University, East Lansing, Michigan 48824*

(Dated: June 27, 2018)

Calculations of the breakup of ^8B and ^{11}Be are performed with the aim of analyzing their sensitivity to the projectile description. Several potentials adjusted on the same experimental data are used for each projectile. The results vary significantly with the potential choice, and this sensitivity differs from one projectile to the other. In the ^8B case, the breakup cross section is approximately scaled by the asymptotic normalization coefficient of the initial bound state (ANC). For ^{11}Be , the overall normalization of the breakup cross section is no longer solely determined by the ANC. The partial waves describing the continuum are found to play a significant role in this variation, as the sensitivity of the phase shifts to the projectile description changes with the physical constraints imposed to the potential.

PACS numbers: 24.10.-i, 25.60.Gc, 25.60.-t, 27.20.+n

Keywords: Coulomb dissociation, asymptotic normalization coefficient, spectroscopic factor, $A = 11$, $A = 8$

I. INTRODUCTION

Since the early days of radioactive beam experiments, breakup reactions have been an important source of information on the structure of nuclei near the dripline. [1, 2, 3, 4, 5]. Usually, the exotic nucleus—the projectile—is simulated by a loosely bound two-body system. The spectroscopic factor of that single-particle wave function is obtained from the comparison of the theoretical predictions with the data [6, 7, 8, 9]. Alternatively, it has been suggested [10, 11] that asymptotic normalization coefficients (ANC) can be obtained from breakup measurements. The basic idea therein is that breakup reactions of loosely bound nuclei are highly peripheral. Since the asymptotic behavior of the projectile wave function is in general well known, the breakup cross section is proportional to the square of the ANC. In this work, we examine the validity of such procedures. We focus on the dependence of the normalization of the Coulomb induced breakup cross section on the single particle potential used for the description of the ground state, as well as the dependence on other features of the projectile, such as excited or scattering states.

There are a variety of state-of-the-art theoretical models to describe a two-body projectile breaking up in the Coulomb and nuclear fields of a target (for a review see [12]). It should be noted that, although there are ways of dealing with three-body projectiles [13, 14] here we will focus on two-body projectiles only. Regardless of the range of applicability, all these reaction models rely on an effective interaction between the two bodies that constitute the nucleus under study. Typically, the geometry of this interaction is fixed (a Woods-Saxon potential with $r_0 \approx 1.2$ fm and $a \approx 0.6$ fm) and the depth is fitted to the binding energy of the projectile taking into account the correct angular momentum and possibly a spin-orbit force. It is clear that this potential is by no means unique and the uncertainty on the potential is expected to have an impact on the normalization of the breakup cross section. Within an effective-range theory, Typel and Baur have indeed shown that the electromagnetic strengths of halo nuclei depend on properties of the two-body projectile description [15, 16]. These include bound-state properties, like the ANC, and parameters that characterize the final state interaction, like the scattering lengths. In Ref. [17], it has also been found that the transfer cross section depend significantly on the single particle parameters. This dependence leads the authors to review the usual method for extracting spectroscopic factors from transfer reactions.

Since the two-body system is loosely bound, one may think that the cross section should scale with the square of the ANC. Many questions remain open: is the reaction sufficiently peripheral for a dependence on ANC? To what extent is this true when couplings in the continuum are important? Or, how does the final state interaction affect the results? In this work we will look at Coulomb breakup from several angles: we study a proton halo ^8B and a neutron halo ^{11}Be , and look at the low energy regime (< 10 MeV/u) versus the higher energy regime (50–100 MeV/u). For this purpose, we use the Continuum Discretized Coupled Channel method [18] or the time-dependent technique

*Electronic address: pierre.capel@centraliens.net

†Electronic address: nunes@nscl.msu.edu

[19], according to applicability and feasibility. Other reaction models like DWBA or first order semiclassical theory [20, 21] are also used as qualitative tools to understand the results. In Sec. II, we present a brief description of the reaction models to be used. In Sec. III, the interactions describing realistic cases are specified as well as other details concerning the calculations. Sec. IV contains the results of the calculations of the Coulomb breakup of ^8B and ^{11}Be . In Sec. V, tests on the sensitivity to the single particle parameters of the projectile are presented and discussed. Finally in Sec. VI, conclusions are drawn.

II. THEORETICAL FRAMEWORK

A. Projectile description

Within the theoretical description of the breakup of a halo nucleus P impinging on a target T , the projectile is usually assumed to have a two-body structure: a pointlike and structureless fragment f (of mass m_f and charge $Z_f e$) loosely bound to a structureless core c (of mass m_c and charge $Z_c e$). The target is described as a structureless particle of mass m_T and charge $Z_T e$. The internal structure of the two-body projectile is described by the Hamiltonian H_0

$$H_0 = -\frac{\hbar^2}{2\mu}\Delta + V_{cf}(\mathbf{r}), \quad (1)$$

where \mathbf{r} is the relative coordinate of the fragment to the core, and $\mu = m_c m_f / (m_c + m_f)$ is the reduced mass of the c - f system. The potential V_{cf} simulates the interaction between the core and the fragment. It is composed of a Coulomb term plus a nuclear term, which comprises a central part and a spin-orbit coupling term

$$V_{cf}(\mathbf{r}) = V_C(r, R_C) + V_0(r) + \mathbf{l} \cdot \mathbf{I} V_{II}(r), \quad (2)$$

where \mathbf{l} is the orbital momentum of the c - f relative motion, and \mathbf{I} is the spin of the fragment. The spin of the core is neglected and assumed to be nil.

The Coulomb term V_C corresponds to the potential due to a uniformly charged sphere of radius R_C (the core) acting on a pointlike particle (the fragment)

$$V_C(r, R_C) = \begin{cases} \frac{1}{2} \frac{Z_c Z_f e^2}{R_C} \left(3 - \frac{r^2}{R_C^2} \right) & r < R_C \\ \frac{Z_c Z_f e^2}{r} & r \geq R_C. \end{cases} \quad (3)$$

The central part of the nuclear potential V_0 has a Woods-Saxon form factor

$$V_0(r) = -V_l f(r, R_0, a), \quad (4)$$

where

$$f(r, R_0, a) = \left[1 + \exp\left(\frac{r - R_0}{a}\right) \right]^{-1}. \quad (5)$$

The spin-orbit coupling term has the usual Thomas form factor

$$V_{II}(r) = V_{IS} \frac{1}{r} \frac{d}{dr} f(r, R_0, a). \quad (6)$$

The radius is parameterized as: $R_0 = r_0 A_c^{1/3}$, where A_c is the mass number of the core. The depths of the potential are adjusted to reproduce the bound states of the system and some of its resonances.

In the lj partial wave, the eigenstates of H_0 are

$$H_0 \phi_{ljm}(E, \mathbf{r}) = E \phi_{ljm}(E, \mathbf{r}), \quad (7)$$

where j is the total angular momentum resulting from the coupling of the orbital momentum l and the fragment spin I , and m is its projection. The negative-energy states correspond either to physical bound states or to Pauli-forbidden states simulating the presence of fragment-like particles in the core. They are normed to unity. The positive energy states describe the continuum of the two-body projectile, i.e. the scattering of the fragment by the core. Their radial part $r^{-1} u_{lj}$ is normalized as

$$u_{lj}(k, r) \xrightarrow{r \rightarrow \infty} [\cos \delta_{lj}(k) F_l(k, r) + \sin \delta_{lj}(k) G_l(k, r)], \quad (8)$$

where $k = \sqrt{2\mu E / \hbar^2}$ is the wave number of the relative motion of the core and the fragment, F_l and G_l are respectively the regular and irregular Coulomb functions [22], and δ_{lj} is the nuclear phase-shift.

B. CDCC

The reaction of a loosely bound two-body projectile on a target can be approximated to a three-body scattering problem. Typically, target excitation is neglected and the three-body wave function is expanded in terms of the intrinsic motion of the core and the fragment $c + f$ within the projectile $u_{lj}(k, r)$, and the motion of the projectile relative to the target $f_{LjJ}(k, R)$. Here \mathbf{R} is the vector connecting the center of mass of the projectile with the target, L is the corresponding orbital angular momentum, and J is the total angular momentum of the system.

For modeling breakup it is important to have a good description of the projectile continuum. One of the most successful methods for elastic breakup is the Continuum Discretized Coupled Channel method (CDCC) [23] first developed for deuteron breakup but today widely applied to exotic nuclei (e.g. [18, 24, 25, 26, 27, 28]). In the standard CDCC, the projectile continuum is included through a discretization into energy bins. For the bin wave function, we use the integral over the momentum interval, weighted by the function g_{lj} in the following way :

$$\tilde{u}_{lj,i}(r) = \sqrt{\frac{2}{\pi N_{lj}}} \int_{k_i}^{k_{i+1}} g_{lj}(k) u_{lj}(k, r) dk . \quad (9)$$

For further details on the normalization N_{lj} of the bins see Ref. [24].

The three-body Schrödinger equation can then be reduced to a coupled channel equation in R ,

$$\left[-\frac{\hbar^2}{2\mu} \left(\frac{d^2}{dR^2} - \frac{L(L+1)}{R^2} \right) + V_{\alpha:\alpha}(R) + E_i - \mathcal{E} \right] f_{\alpha J}(R) = \sum_{\alpha' \neq \alpha} i^{L'-L} V_{\alpha:\alpha'}^J(R) f_{\alpha' J}(R), \quad (10)$$

where the subscript α represents all relevant quantum numbers and E_i is the average energy of continuum bin $[k_i, k_{i+1}]$ (or $E < 0$ for the bound states), and \mathcal{E} is the total energy of the system. The coupling potential $V_{\alpha:\alpha'}^J(R)$ consists of the sum of the core-target and fragment-target interactions averaged over the projectile states [29]. One can solve Eq. (10) exactly: the solution Ψ^{CDCC} includes all possible rearrangements within the projectile continuum. One can also solve Eq. (10) iteratively: the one-step iteration of Eq. (10) is equivalent to the standard DWBA, where the optical potential between the projectile and the target is replaced by the folding potential $V_{0:\alpha'}^J(R)$ [30].

C. Time-dependent model

The time-dependent description of the reaction [19, 31, 32, 33, 34, 35, 36] relies on the semiclassical approximation [20, 21] in which the projectile-target relative motion is treated classically, while the internal motion of the projectile is described quantum mechanically. The target is assumed to follow a classical trajectory in the projectile rest frame. The projectile is therefore seen as evolving in a time-dependent potential which simulates its interaction with the target. The wave function Ψ describing its internal structure is solution of the following time-dependent Schrödinger equation

$$i\hbar \frac{\partial}{\partial t} \Psi(\mathbf{r}, t) = [H_0 + V(\mathbf{r}, t)] \Psi(\mathbf{r}, t), \quad (11)$$

where H_0 [see Eq. (1)] describes the internal structure of the projectile, and V is the time-dependent potential that simulates the P - T interaction. The latter reads

$$V(\mathbf{r}, t) = V_{cT}[r_{cT}(t)] + V_{fT}[r_{fT}(t)] - \frac{(Z_c + Z_f)Z_T e^2}{R(t)}, \quad (12)$$

where the time-dependent coordinate \mathbf{R} describes the classical trajectory followed by the target in the projectile rest frame. It is a hyperbola, which can be approximated fairly well by a straight line at high energies. The vectors \mathbf{r}_{cT} and \mathbf{r}_{fT} correspond respectively to the core-target and fragment-target coordinates. In Eq. (12), V_{cT} and V_{fT} are local potentials which model the interaction between the target and the projectile constituents. They comprise a Coulomb term and a short-range optical potential, which simulates the nuclear interaction.

Eq. (11) is solved numerically considering the projectile initially in its ground state $\phi_{l_0 j_0 m_0}$ of energy E_0 . We use the algorithm described in Ref. [19], and consider linear trajectories. For each trajectory, characterized by impact parameter b , we deduce the breakup probability P_{bu} by projecting the output wave function $\Psi(\mathbf{r}, t \rightarrow +\infty)$ onto the positive eigenstates of H_0 , which describe the projectile after dissociation. The breakup cross section σ_{bu} is then obtained by summing this probability over all impact parameters.

Potential	V_l (MeV)	V_{lS} (MeV fm ²)	a (fm)	r_0 (fm)
T1	45.23	19.59	0.40	1.25
T2	44.98	19.59	0.52	1.25
T3	44.47	19.59	0.60	1.25
T4	43.50	19.59	0.70	1.25
T5	42.28	19.59	0.80	1.25

TABLE I: Parameters of the ${}^7\text{Be}$ - p potentials [see Eqs. (2)-(6)]. Note that R_0 used in (3)-(6) is parameterized as $r_0 A_c^{1/3}$, and the Coulomb radius is always kept constant at $R_C = 1.3 A_c^{1/3}$ fm.

Potential	$E_{0p3/2}$ (MeV)	$b_{0p3/2}$ (fm ^{-1/2})	$E_{0p1/2}$ (MeV)	$\Gamma_{0p1/2}$ (MeV)
T1	-0.137	0.6477	2.8	2.2
T2	-0.137	0.7008	2.3	1.6
T3	-0.137	0.7410	1.9	1.2
T4	-0.137	0.7959	1.6	0.9
T5	-0.137	0.8554	1.3	0.7

TABLE II: Levels obtained with the five potentials listed in Table I. The energies and widths are expressed in MeV. The ANC of the $0p3/2$ ground state $b_{0p3/2}$ is displayed as well.

At sufficiently high energies, the solution of Eq. (11) can be approximated by first-order perturbation theory [20, 21]. In that approximation the breakup process is assumed to occur in one step from the initial ground state to the continuum, and the couplings inside the continuum are neglected. The first-order approximation of the breakup cross section reads

$$\frac{d\sigma_{\text{bu}}^{(1)}}{dE}(E) = \frac{1}{\hbar^2} \frac{2\pi}{2j_0 + 1} \sum_{m_0} \sum_{l_{jm}} \int \left| \left\langle \phi_{l_{jm}}(E, \mathbf{r}) \left| \int_{-\infty}^{\infty} e^{i\omega t} V(\mathbf{r}, t) dt \right| \phi_{l_0 j_0 m_0}(E_0, \mathbf{r}) \right\rangle \right|^2 db, \quad (13)$$

where $\omega = (E - E_0)/\hbar$.

When the projectile-target interactions are purely Coulomb, the first-order approximation of the breakup probability can be easily expressed as a series of the contributions of each multipole of the time-dependent potential (11). In practice, only the first terms of that series are needed. For straight-line trajectories, a semi-analytical expression of the dipole and quadrupole contributions to the first-order breakup probability can be obtained (see e.g. Ref. [37]).

III. TWO-BODY INTERACTIONS

A. Description of ${}^8\text{B}$

The ${}^8\text{B}$ nucleus is described by the usual two-body system: a proton loosely bound to a ${}^7\text{Be}$ core in its $\frac{3}{2}^-$ ground state [24, 33, 38, 39, 40]. The internal structure of the core is neglected, and its spin is set to zero in the calculations. The 2^+ ground state of ${}^8\text{B}$ is assumed to be a pure $p3/2$ proton single-particle state. As explained in Sec. II A, the interaction between the core and the proton is simulated by a local potential [see Eqs. (2)-(6)].

In order to study the sensitivity of the calculations to the description of the projectile, five ${}^7\text{Be}$ - p potentials are considered. The parameters of these potentials are listed in Table I. They are obtained by varying the diffuseness of a simplified version of the potential developed by Esbensen and Bertsch [33] (potential T2). While the spin-orbit term is kept unchanged for all potentials, the depth of the central part V_l is adjusted to reproduce the 137 keV binding energy of the bound state [41]. Since the spin of the core is neglected, the 0^+ , 1^+ , and 3^+ states resulting from the coupling of this $\frac{3}{2}$ spin and the $\frac{3}{2}$ angular momentum of the halo proton are degenerate with the 2^+ ground state. Therefore, the p -wave 1^+ resonance at $E = 0.63$ MeV [41] is not reproduced by this parameterization. We use the same potential for all partial waves. The levels obtained with the potentials of Table I are listed in Table II. The ANC of the ground state $b_{0p3/2}$ is given as well. Note that besides the $0p3/2$ ground state, the potentials exhibit also a $p1/2$ resonance, which does not correspond to any known physical state. This unphysical state has not been adjusted, and its energy varies from one potential to the other.

Potential	V_{even} (MeV)	V_{odd} (MeV)	V_{IS} (MeV fm ²)	a (fm)	r_0 (fm)
V1	62.52	39.74	21.0	0.6	1.2
V2	66.325	38.37	12.44	0.5	1.2
V3	58.905	40.025	27.68	0.7	1.2
V4	71.28	49.015	29.95	0.6	1.1
V5	55.25	32.515	12.86	0.6	1.3
V6	59.05	59.05	0	0.62	1.236

TABLE III: Parameters of the ^{10}Be - n potentials [see Eqs. (2)-(6)]. Note that R_0 used in (3)-(6) is parameterized as $r_0 A_c^{1/3}$.

Potential	$E_{1s1/2}$ (MeV)	$b_{1s1/2}$ (fm ^{-1/2})	$E_{0p1/2}$ (MeV)	$E_{0d5/2}$ (MeV)	$\Gamma_{0d5/2}$ (MeV)
V1	-0.504	0.83	-0.184	1.274	0.162
V2	-0.504	0.80	-0.184	1.274	0.131
V3	-0.504	0.87	-0.184	1.274	0.200
V4	-0.504	0.82	-0.184	1.274	0.145
V5	-0.504	0.85	-0.184	1.274	0.181
V6	-0.504	0.85	-12.5	2.6	0.9

TABLE IV: Levels obtained with the six potentials listed in Table III. Potentials V1 to V5 were adjusted to the first three levels of ^{11}Be , while V6 reproduces only the $\frac{1}{2}^+$ ground state. The ANC of the $1s1/2$ state is displayed as well.

B. Description of ^{11}Be

As in previous studies [19, 31, 32, 34, 36, 42, 43, 44], ^{11}Be is described as a neutron loosely bound to a ^{10}Be core. The ^{10}Be core is assumed to be in its 0^+ ground state. The depths of the V_{cf} potential (2) simulating the interaction between ^{10}Be and the neutron are adjusted to reproduce the low-lying levels in the ^{11}Be spectrum [45]. The well known shell inversion observed between the two bound states of ^{11}Be is reproduced using a parity dependent depth of the central term of the nuclear potential V_I . The $\frac{1}{2}^+$ ground state is modeled by a $1s1/2$ state, the $\frac{1}{2}^-$ excited state by a $0p1/2$ state, and the $\frac{5}{2}^+$ resonance is adjusted in the $d5/2$ partial wave.

In this case, we make use of six sets of parameters to study the sensitivity of our calculations to the potential choice. They are listed in Table III. The first potential (V1) was developed for a time-dependent analysis of the breakup of ^{11}Be on ^{12}C [44]. The next four (V2 to V5) have been derived from V1 by varying either the diffuseness or the radius of the Woods-Saxon form factor [46]. The values were chosen to encompass those used in most other breakup calculations [31, 32, 36, 42]. In addition, we also use a sixth potential (V6) developed by Fukuda *et al.* for analyzing their data [9]. It reproduces only the ground state energy of ^{11}Be and does not include a spin-orbit coupling term.

The physical energy levels obtained with these six potentials are listed in Table IV. The asymptotic normalization coefficient $b_{1s1/2}$ of the ground state is also given.

C. Projectile-target interactions

The reactions we consider are Coulomb dominated. However, the nuclear interactions between the target and the projectile composites are not negligible [19, 24]. As mentioned earlier, they are simulated by short ranged optical potentials. The general form factor of the potential simulating the interaction between the constituent x and the target T is

$$V_{xT}(r) = V_C(r, R_C) - Vf(r, R_R, a_R) - iWf(r, R_I, a_I) - iW_{DAI} \frac{d}{dr} f(r, R_I, a_I), \quad (14)$$

where V_C is the point-sphere Coulomb potential (3), and f is the Woods-Saxon form factor (5). The values of the parameters we consider for these interactions are listed in Table V. They correspond to potentials found in the literature for similar systems.

As in Ref. [24], we simulate the interaction between ^7Be and ^{58}Ni at low energy using the potential developed by Moroz *et al.* [47]. This potential reproduces elastic scattering data of ^7Li impinging on ^{58}Ni at 14.2 MeV.

To model the interaction between ^{10}Be and ^{208}Pb at 69 MeV per nucleon, as in Ref. [19], we follow Typel and Shyam [42] and adapt a potential developed by Bonin *et al.* [48], which reproduces the elastic scattering cross section of α on lead at 699 MeV.

x	T	Energy (MeV/nucleon)	V (MeV)	R_R (fm)	a_R (fm)	W (MeV)	W_D (MeV)	R_I (fm)	a_I (fm)	R_C (fm)
${}^7\text{Be}$	${}^{58}\text{Ni}$	3	100	4.064	0.65	30.6	0	4.347	0.80	5.032
${}^{10}\text{Be}$	${}^{208}\text{Pb}$	69	70.0	7.43	1.0	58.9	0	7.19	1.04	5.92
p	${}^{58}\text{Ni}$	3	54.512	4.529	0.75	0	11.836	4.877	0.58	5.032
n	${}^{208}\text{Pb}$	69	29.46	6.93	0.75	13.4	0	7.47	0.58	-

TABLE V: Parameters of the optical potentials (14) which simulate the interaction between the projectile constituents and the targets.

The interactions of the valence nucleon with the targets are approximated by the parameterization of Becchetti and Greenlees [49], as in previous works [19, 24].

IV. BREAKUP CALCULATIONS

A. The ${}^8\text{B}$ case

The breakup of ${}^8\text{B}$ on ${}^{58}\text{Ni}$ has been measured at 25.75 MeV at Notre-Dame [50, 51]. This reaction is analyzed in Ref. [24] within the CDCC framework (see Sec. II B). The calculation is in good agreement with the data using the two-body description of ${}^8\text{B}$ given in Sec. III A (potential T2 of Table I).

In the present paper, we study the sensitivity of this analysis to the ${}^7\text{Be}$ - p potential choice. CDCC calculations identical to that of Ref. [18] are performed with the code FRESKO [52] considering the five potentials T1–T5 listed in Table I. For the model space, we use L up to 1000, a maximum radius for the distorted waves of $R_{\text{max}} = 500$ fm and coupling potentials truncated at $R_{\text{bin}} = 60$ fm. The discretization of the continuum of the projectile is made up to $E_{\text{max}} = 4$ MeV and all dipole and quadrupole transitions for s, p and d waves are included. As in Ref. [18], the nuclear interactions between the projectile constituents and the nickel target are simulated by the optical potentials given in Table V.

First, let us consider simpler cases of the continuum wave functions whilst changing the ground state interaction according to models T1–T5. If only pure Coulomb waves are taken in the ${}^7\text{Be}$ - p continuum, the scaling with the square of the ANC of the initial bound state $b_{0p3/2}$ is perfect (i.e. with less than 1 % difference). This same result is obtained if the nuclear scattering ${}^7\text{Be}$ - p potential is kept fixed to T1 for all models. We have checked these results using other reaction models. The DWBA approximation leads to the same conclusion, as well as the first-order approximation when the breakup of ${}^8\text{B}$ on ${}^{58}\text{Ni}$ is computed at higher energy (50 MeV/nucleon) considering a purely Coulomb interaction between the projectile and the target. The direct proportionality of the cross section to the square of the ANC of the initial bound state indicates that only the asymptotic part of the wave function has an influence upon the cross section, consistent with the small binding energy of the projectile.

When the scattering potential is chosen to correspond to the ground-state interaction, the breakup cross section is only approximately proportional to $b_{0p3/2}^2$. This is illustrated in Fig. 1, where the breakup cross sections obtained with potentials T1–T5 are plotted as a function of the relative energy between the ${}^7\text{Be}$ core and the proton after breakup. To emphasize the sensitivity to the potential choice, those values are divided by the square of the ANC. The different curves exhibit similar behaviors. They all increase sharply to reach a maximum around 0.5 MeV, and display a bump in the slow decrease that follows the maximum. However, these behaviors are not identical. First, even though they have been divided by $b_{0p3/2}^2$, their magnitudes differ by approximately 4 % in the vicinity of the maximum. Second, the location of the bump changes with the potential choice. Since these features do not appear when the same scattering potential is used, they are due to differences in the distorted waves.

To understand these features, we analyze the contributions of the different partial waves to the breakup cross section. The sensitivity of these contributions to the potential choice vary from one partial wave to the other. This is illustrated in Fig. 2, which displays the $p3/2$ (dominant) and the $p1/2$ contributions to the cross section. They both have been divided by $b_{0p3/2}^2$. On the one hand, the $p3/2$ contributions—as well as the s and d ones—exhibit very similar shapes, but their magnitudes vary by 4 %—this variation goes up to 8 % for the s component. These results explain the non exact proportionality of the total breakup cross section to the square of the single particle ANC. On the other hand, each $p1/2$ contribution exhibits a maximum whose location varies with the potential choice. These maxima are responsible for the presence of the bumps in the total cross sections above 1 MeV. They are related to the $p1/2$ resonance obtained with potentials T1–T5 (see Table II). This effect has already been observed in the breakup of ${}^{11}\text{Be}$ on ${}^{12}\text{C}$, where the presence of the $\frac{5}{2}^+$ resonance in the ${}^{11}\text{Be}$ spectrum induces a narrow peak in the cross section [9, 44]. It confirms that the description of the continuum has a significant influence on the breakup calculation.

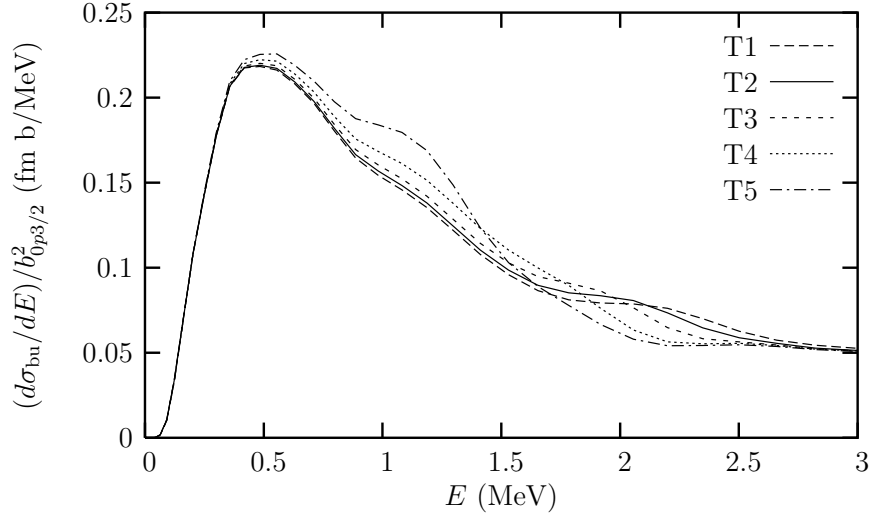


FIG. 1: Cross section for the breakup of ${}^8\text{B}$ on ${}^{58}\text{Ni}$ at 25.75 MeV divided by the square of the single particle ANC. The cross section is given as a function of the ${}^7\text{Be}$ - p relative energy E after breakup. Calculations are performed with the different ${}^7\text{Be}$ - p potentials listed in Table I.

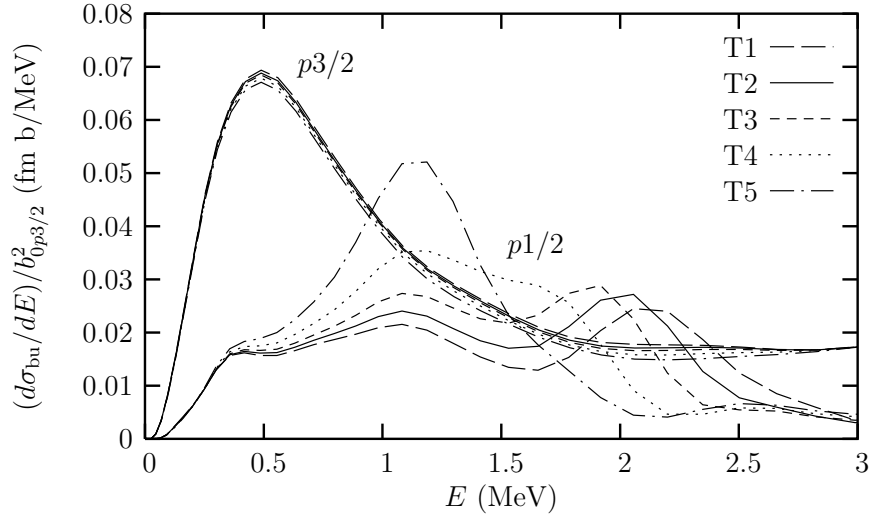


FIG. 2: Contributions of $p3/2$ and $p1/2$ partial waves to the breakup cross section of ${}^8\text{B}$ on ${}^{58}\text{Ni}$. They are plotted as a function of E , and are divided by the square of the single particle ANC. Calculations are performed with the different ${}^7\text{Be}$ - p potentials listed in Table I.

The same effects are observed in DWBA calculations, and, at higher energy (50 MeV/nucleon), within the first-order perturbation theory. However, since the contribution of the E2 component decreases at high energy, the sensitivity to the p -wave continuum is less noticeable in the latter case.

These results indicate that the breakup calculations are sensitive, not only to the tail of the ground-state wave function, but also to the way the continuum of the projectile is described. This influence of the continuum description upon breakup calculations has already been mentioned in Ref. [11]. In that reference, Trache *et al.* observed that the momentum distributions computed using distorted waves differed from those obtained previously with plane waves [10]. Since the reaction is very peripheral, the sensitivity to the scattering potential is most likely due to the subsequent variations in the phase shifts. The detailed analysis of these effects is addressed in Sec. V.

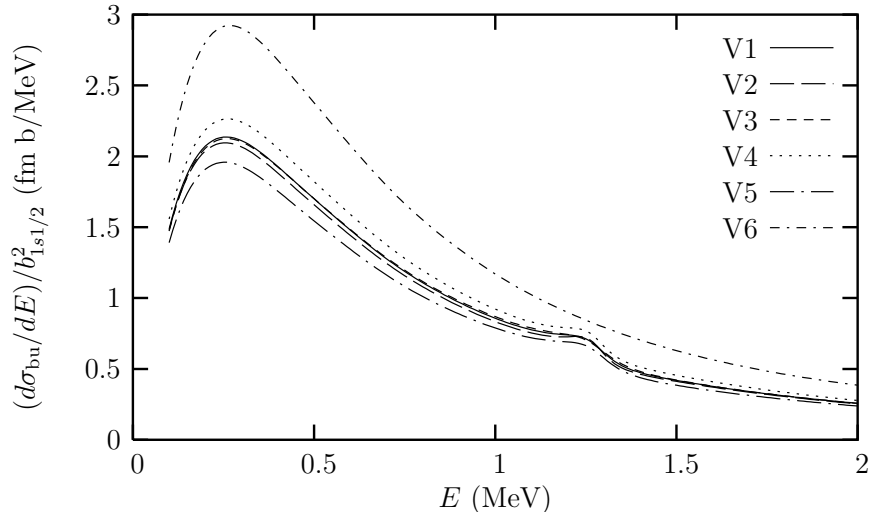


FIG. 3: Breakup cross section of ^{11}Be on ^{208}Pb at 69 MeV/nucleon as a function of the energy E . The value is divided by the square of the single particle ANC. Calculations are performed with potentials V1–V6 listed in Table V.

B. The ^{11}Be case

A more severe case of the breakdown of the ANC scaling is found in the Coulomb breakup of ^{11}Be on lead. This reaction has recently been measured at RIKEN at 69 MeV/nucleon [9]. From the analysis of their experiment, Fukuda *et al.* extracted a spectroscopic factor of about 0.7 for the $|^{10}\text{Be}(0^+) \otimes s1/2\rangle$ configuration of the ground state of ^{11}Be .

With the aim of analyzing the sensitivity of this figure to the $^{10}\text{Be}-n$ potential, we perform time-dependent calculations of the reactions using the six potentials V1–V6 described in Sec. III B. As in Ref. [19], the calculations are done within the time-dependent framework described in Sec. II C using the optical potentials listed in Table V for simulating the nuclear interactions between the projectile and the target.

As for ^8B , if simplifications are performed in the continuum (namely, switching off the nuclear Be- n interaction, or taking the same interaction for all scattering partial waves as the ground state), the resulting breakup cross section is directly proportional to the square of the ground state ANC $b_{1s1/2}^2$. When the realistic ^{11}Be interactions of table II are used, the situation changes: the cross section is no longer proportional to $b_{1s1/2}^2$. This is illustrated in Fig. 3, where the breakup cross sections divided by $b_{1s1/2}^2$ are plotted as a function of the relative energy between the ^{10}Be core and the neutron after breakup. All curves exhibit the same shape—if one excepts the small bump around 1.3 MeV due to the $d5/2$ resonance, which is not reproduced by the potential V6. However, their magnitude varies significantly from one potential to the other. In particular, V6 leads to a cross section larger by 40 % than V1–V5. Moreover, even though they have been adjusted on the same energy levels, these five potentials lead to variations in the breakup cross sections as large as 20 %. Since this discrepancy is observed only when the scattering potential differs, we conclude that the way the continuum is described has a significant influence on the breakup calculation. The same result is obtained within the first-order approximation. With such a variation of the calculation with the potential choice, the validity of the spectroscopic factor extracted by Fukuda *et al.* from their breakup measurement [9] is questionable.

The effect observed in Fig. 3 is very different from one partial wave to the other. This is illustrated in Fig. 4, where the dominant $p3/2$ and $p1/2$ contributions to the total cross section are depicted. Like the results shown in Fig. 3, they have been divided by $b_{1s1/2}^2$ to cancel the dependence on the ANC. On the one hand, the difference between V1–V5 is located mainly in the $p3/2$ contribution. These potentials lead indeed to very similar $p1/2$ contributions. On the other hand, even if the $p3/2$ contribution of potential V6 is still higher than that of the others, the major difference between that potential and the other five lies mainly in the $p1/2$ contribution. This partial wave analysis confirms that the breakup cross section depends not only on the ground-state wave function, but also on the description of the partial waves describing the continuum.

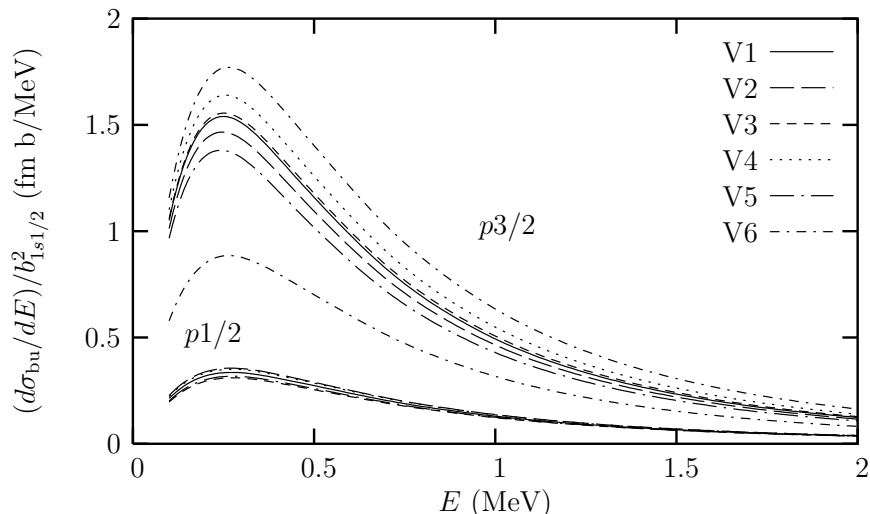


FIG. 4: Contributions of the main partial waves $p3/2$ and $p1/2$ to the breakup cross section of ^{11}Be on ^{208}Pb . The values are divided by the square of the single particle.

V. ANALYSIS OF THE SENSITIVITY TO THE POTENTIAL CHOICE

The features presented in the previous section are all reproduced using fully coupled reaction models (like CDCC or time-dependent approaches) and also one-step approximations (like DWBA or first-order perturbation theory). This indicates that those dependences appear mainly through first-order transitions from the initial bound state to the continuum. Therefore, higher-order effects will be neglected in the qualitative analysis presented in this section. The effects observed in section IV can be explained through the study of the wave functions of the initial bound states and those of the partial waves describing the continuum [see Eq. (13)]. Since for both nuclei the breakup reaction is Coulomb dominated, we neglect the nuclear contribution in the following qualitative analysis and consider only the Coulomb potential, which we expand into multipoles.

The contributions of the p waves to the breakup of ^8B on ^{58}Ni displayed in Fig. 2 correspond mainly to E2 transitions from the ground state. These transitions are large because the reaction occurs at low energy. Fig. 5 pictures the radial wave functions of the ground state (a) and the continuum states, $p3/2$ (b) and $p1/2$ (c), computed at an energy of 1 MeV.

Once divided by their ANC, the wave functions of the ^8B ground state obtained with the different $^7\text{Be}-p$ potentials are identical above 5 fm [Fig. 5(a)]. The only difference between them lies below that radius. Due to the low binding energy of the system, these wave functions exhibit a very long range. This long range, and the presence of the r^2 factor of the quadrupole term of the Coulomb potential in the transition matrix element ensures the peripherality of the breakup reaction. Consequently, the breakup cross sections are not very sensitive to the differences at small radius. This explains why, when the same description of the continuum is chosen in all calculations, the cross section is exactly proportional to $b_{0p3/2}^2$. If the continuum is described using potentials T1–T5, the corresponding wave functions differ from one potential to the other. Since the reaction is very peripheral, only the differences in the distorted waves for $r \geq 5$ fm (i.e. mainly phase shifts) lead to variations in the breakup cross sections. This difference is illustrated in part (b) of Fig. 5 for the dominant $p3/2$ partial wave. Potentials T1–T5 indeed lead to variations in the phase shift of the wave function. These remain small though due to the fact that all potentials have been adjusted to reproduce the low-lying ground state in that partial wave. However, they are not negligible, and explain the loss of exact proportionality of the $p3/2$ contribution to the breakup cross section to the square of the ANC, illustrated in Fig. 2. A similar analysis of the s and d continuum wave functions explains the lack of proportionality to $b_{0p3/2}^2$ of these components as well.

The differences between the $p1/2$ partial waves are much more significant [Fig. 5(c)]. This is due to the presence in that partial wave of a low-lying resonance whose energy varies from one potential to the other (see Table II). These large variations account for the significant distortions shown in Fig. 2.

In the case of the Coulomb breakup of ^{11}Be at 69 MeV/nucleon the same reasoning can be done in order to explain the significant variations observed in Fig. 3. Occurring at higher energy, the transition to the continuum is dominated by the E1 term of the Coulomb interaction [37]. Therefore, starting from an initial s state, the transfer to the continuum occurs mainly through p waves.

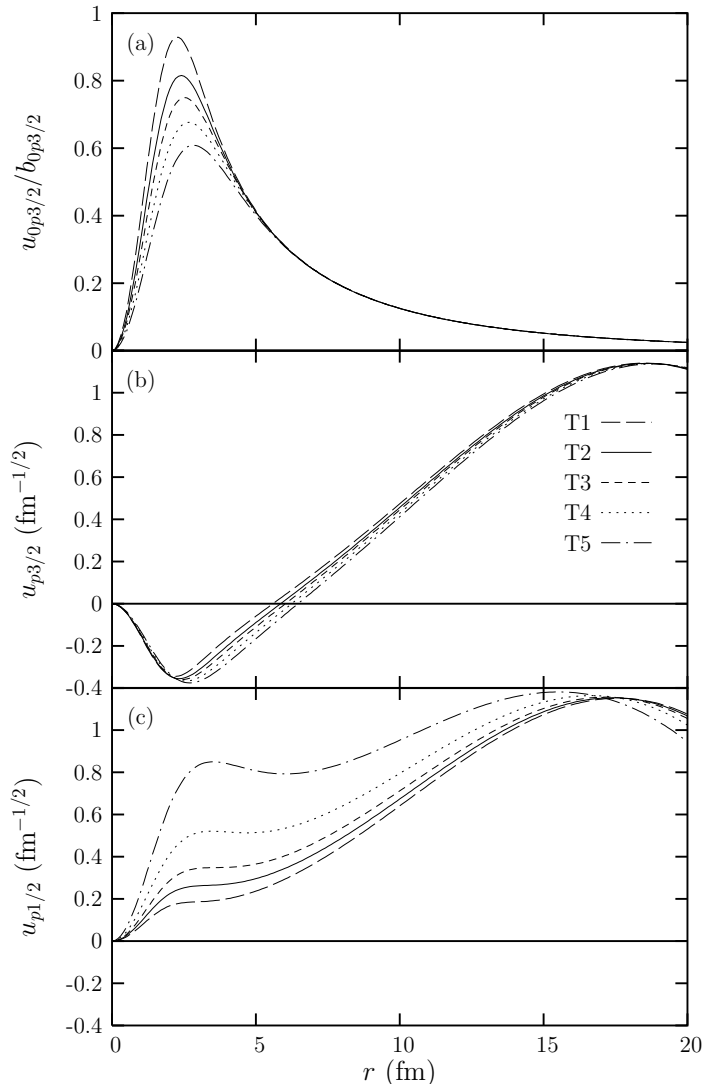


FIG. 5: Wave functions of ${}^8\text{B}$ obtained with the different ${}^7\text{Be}$ - p potentials T1–T5: (a) the initial ground state divided by $b_{0p3/2}$, (b) and (c) the $p3/2$ and $p1/2$, respectively, continuum wave functions computed at $E = 1$ MeV.

Fig. 6 depicts the radial wave functions of the initial $1s1/2$ ground state (a), and of the $p3/2$ (b) and $p1/2$ (c) scattering states at $E = 1$ MeV. They are calculated for the potentials V1–V6 of Table III. As in Fig. 5(a), the ground state wave function is divided by the ANC. As in the ${}^8\text{B}$ case, due to the long range of the wave function, and to the r factor appearing in the matrix element, the first order breakup cross section is not sensitive to the variations at small radii. The cross section should therefore be proportional to $b_{1s1/2}^2$. However, as for ${}^8\text{B}$, the change in the potential leads also to variations in the scattering wave functions. In the present case, though, the changes in the dominant component are much more significant than in the previous example, explaining the large differences observed in the breakup cross section in Sec. IV B. We indeed observe significant variations in the $p3/2$ phase shift [Fig. 6(b)]. These variations are responsible for the large differences in the $p3/2$ contribution to the breakup cross section observed in Fig. 4. They overcome by far the differences due to the ANC, which means that the ${}^{11}\text{Be}$ breakup reaction of Ref. [9] seems more sensitive to the way its continuum is described than to the details of its initial single particle state.

The differences observed in the $p1/2$ contribution to the cross section (Fig. 4) can easily be understood by the variations in the phase shift shown here. The very similar $p1/2$ phase shifts obtained with potentials V1–V5 justify that these five potentials lead to approximately the same $p1/2$ contributions to $(d\sigma/d\Omega)/b_{1s1/2}^2$. The similarity in the $p1/2$ phase shifts is due to the fact that all those potentials have been adjusted in order to reproduce the very loosely bound $\frac{1}{2}^-$ excited state of ${}^{11}\text{Be}$ in that partial wave. Potential V6, that does not reproduce this excited state,

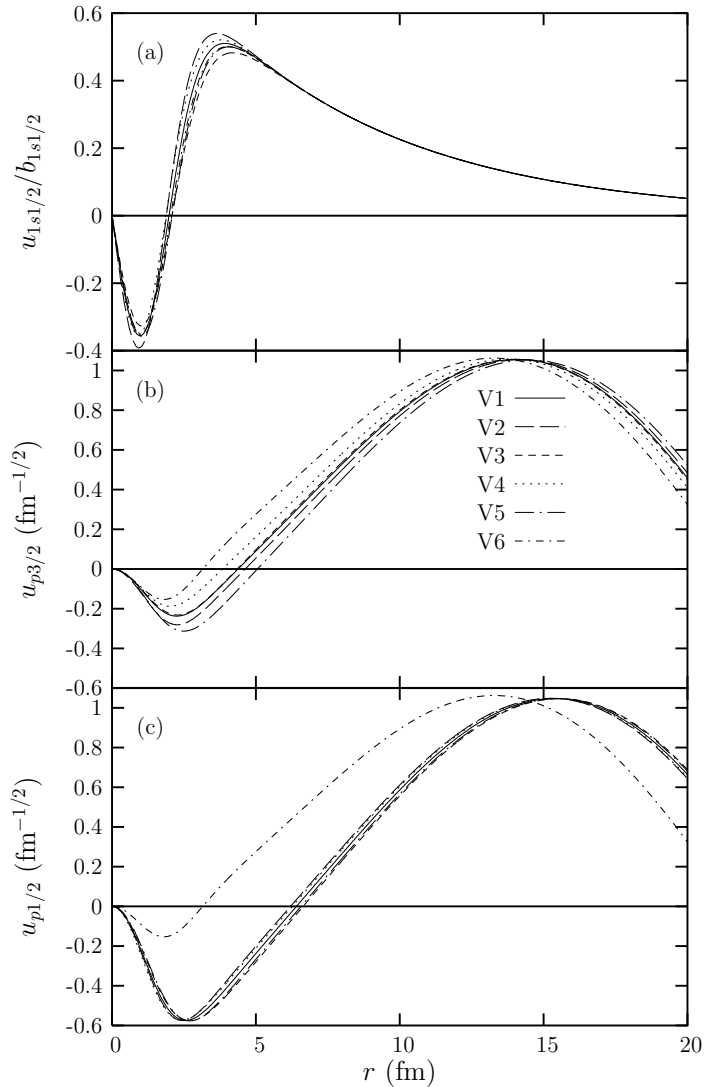


FIG. 6: Wave functions of ^{11}Be obtained with the different ^{10}Be - n potentials V1-V6: (a) the initial ground state divided by $b_{1s1/2}$, (b) and (c) the $p_{3/2}$ and $p_{1/2}$, respectively, continuum wave functions computed at $E = 1$ MeV.

presents a very different phase shift of the $p_{1/2}$ component, which explains its larger $p_{1/2}$ contribution to the cross section.

This first-order analysis of the breakup reactions explains qualitatively the sensitivity of our calculations to the core-fragment potential. It shows that the wave functions describing both the ground state and the continuum have a significant influence on the cross section. Since the reaction is mostly peripheral, this influence occurs mainly through the asymptotic characteristics of the wave functions, i.e. the ANC of the initial bound state, and the phase-shift in the continuum.

These results confirm the study of the electromagnetic strengths in one-nucleon halo nuclei performed by Typel and Baur in Ref. [16]. In that paper, the authors analyze the sensitivity of $B(E\lambda)$ transitions to the two-body description of the loosely-bound nuclei. They show that the energy distributions depend not only on the description of the bound state, but also on that of the continuum. Assuming the actual wave functions can be replaced by their asymptotic behaviours, they obtain simple analytical expressions for the energy distributions. These expressions show clearly that the transition strengths can be characterized by only a few parameters describing the nucleus: the binding energy of the system, the ANC of the bound state wave function, and the scattering length describing the final state interaction. The present analysis shows that these conclusions remain qualitatively valid in breakup reactions where higher-order effects and nuclear interactions are significant [24, 37].

It should be noted that the shape of the transition strengths obtained by Typel and Baur depends significantly

on the scattering length (see Figs. 9 and 10 of Ref. [16]). If this were so, it should enable the extraction of the ANC and the scattering length from the same data. However, our results show hardly any distortion of the breakup cross sections with the potential choice. The curves differ only in amplitude, not in shape, even though the various potentials lead to significantly different phase shifts. The consequence is then that the final state interaction needs to be constrained by other observables in addition to the breakup energy distribution. This discrepancy between our results and those of Ref. [16] is due to further approximations performed in Ref. [16] required for obtaining analytic solutions. We find that the analytic expressions of Ref. [16] are only useful qualitatively. The shape and peak of the energy distributions are not correctly produced.

VI. CONCLUSION

In this paper, the breakup calculations of two loosely bound projectiles, ${}^8\text{B}$ and ${}^{11}\text{Be}$, have been performed within CDCC and time-dependent frameworks at low and high energy, respectively. Different potentials were used to simulate the interaction between both constituents of the projectile. It has been shown that the potential geometry has a significant influence upon the breakup cross section. This dependence occurs through the asymptotic normalization coefficient of the initial bound state, as expected from the peripheral nature of the reaction. However, the way excited states and the continuum are modeled also plays a role.

These results have been confirmed using DWBA and/or first-order perturbation theory. These approximations enabled us to interpret the variations observed in the more elaborated techniques with one-step theory. Our analysis shows with transparency that different potential geometries lead to differences in the phase shifts that can affect significantly the total cross section. This qualitative analysis is in good agreement with Typel and Baur's analytical study of the electromagnetic strengths in halo nuclei [16].

One of our test cases consisted of the breakup of ${}^8\text{B}$ on ${}^{58}\text{Ni}$ at 25.75 MeV. Different potentials lead to minor variations in the dominant $p3/2$ phase shift, since all potentials have been adjusted to reproduce the ${}^8\text{B}$ ground state in that partial wave. These variations induce only 4 % differences in the breakup cross section, which remains therefore approximately proportional to the square of the ANC. On the contrary, our potentials give large differences in the $p1/2$ phase shift, leading to significant distortion in the energy distribution for this partial wave. As this partial wave is less important in this reaction, the phase shift differences have a smaller effect in the normalization of the total cross section.

In the breakup of ${}^{11}\text{Be}$ on ${}^{208}\text{Pb}$ at 69 MeV/nucleon, no fitting was imposed on the dominant $p3/2$ partial wave, thus the various potentials lead to significant differences in the corresponding phase shifts. These differences are so large that they overcome those in the single particle ANC. The cross section is therefore not proportional to the square of the ANC. Five out of the six potentials we have used for this analysis have been adjusted to reproduce the $\frac{1}{2}^-$ excited state of ${}^{11}\text{Be}$ in the $p1/2$ partial wave. This induces very similar phase shifts in that partial wave. That contribution to the cross section is therefore nearly proportional to the square of the ANC. A sixth potential, that does not reproduce the excited state, has a very different $p1/2$ phase shift, and leads to a much higher $p1/2$ contribution.

These results show that Coulomb breakup reactions probe not only the ground state of the projectile, as it is usually assumed, but also the continuum description. We have indeed seen that differences in the phase shift of the dominant partial wave can influence significantly breakup calculations. Therefore, one should be particularly cautious when extracting ground-state spectroscopic information or ANCs from breakup measurements. As shown in the calculation of the Coulomb breakup of ${}^{11}\text{Be}$, different descriptions of the continuum can lead to variations in the cross section up to 40 %, generating a significant inaccuracy in the spectroscopic factor. Moreover, even though the reaction is very peripheral, the extraction of the single-particle ANC from breakup measurements can be very tricky due to the strong dependence of the calculations on the scattering waves. The sensitivity of the extracted values to the potential geometry should therefore be evaluated, and taken into account in the analysis. Whenever possible, the potentials used to simulate two-body projectiles should be adjusted on other experimental data (excited states and phase shifts). This underlines the need for additional data to constrain the scattering properties of the core-fragment potentials.

Acknowledgments

We would like to thank A. M. Mukhamedzhanov for useful comments to the manuscript, and D. Baye for interesting discussions on this work. P. C. acknowledges the support of the Natural Sciences and Engineering Research Council of Canada (NSERC). Support from the NSCL at Michigan State University and from the National Science Foundation

grant PHY-0456656 is acknowledged.

-
- [1] P. G. Hansen, A. S. Jensen, and B. Jonson, *Ann. Rev. Nucl. Part. Sci.* **45**, 591 (1995).
 - [2] I. Tanihata, *J. Phys. G* **22**, 157 (1996).
 - [3] G. Baur, K. Hencken, and D. Trautmann, *Prog. Part. Nucl. Phys.* **51**, 487 (2003).
 - [4] B. Jonson, *Phys. Rep.* **389**, 1 (2004).
 - [5] G. Baur and H. Rebel, *Ann. Rev. Nucl. Part. Sci.* **46**, 321 (1996).
 - [6] T. Nakamura *et al.*, *Phys. Lett. B* **331**, 296 (1994).
 - [7] R. Palit *et al.*, *Phys. Rev. C* **68**, 034318 (2002).
 - [8] U. D. Pramanik *et al.*, *Phys. Lett. B* **551**, 63 (2003).
 - [9] N. Fukuda *et al.*, *Phys. Rev. C* **70**, 054606 (2004).
 - [10] L. Trache, F. Carstoiu, C. A. Gagliardi, and R. E. Tribble, *Phys. Rev. Lett.* **87**, 271102 (2001).
 - [11] L. Trache, F. Carstoiu, C. A. Gagliardi, and R. E. Tribble, *Phys. Rev. C* **69**, 032802(R) (2004).
 - [12] J. Al-Khalili and F. M. Nunes, *J. Phys. G* **29**, R89 (2003).
 - [13] J. A. Christley, J. S. Al-Khalili, J. A. Tostevin, and R. C. Johnson, *Nucl. Phys. A* **624**, 275 (1997).
 - [14] M. Kamimura, in *Proceedings of the Second Argonne/MSU/JINA/INT RIA Workshop on Reaction Mechanisms for Rare Isotope Beams*, edited by B. A. Brown (American Institute of Physics, New-York, 2005), (to be published).
 - [15] S. Typel and G. Baur, *Phys. Rev. Lett.* **93**, 142502 (2004).
 - [16] S. Typel and G. Baur, *Nucl. Phys. A* **759**, 247 (2005).
 - [17] A. M. Mukhamedzhanov and F. M. Nunes, *Phys. Rev. C* **72**, 017602 (2005).
 - [18] F. M. Nunes and I. J. Thompson, *Phys. Rev. C* **59**, 2652 (1999).
 - [19] P. Capel, D. Baye, and V. S. Melezhik, *Phys. Rev. C* **68**, 014612 (2003).
 - [20] K. Alder *et al.*, *Rev. Mod. Phys.* **28**, 432 (1956).
 - [21] K. Alder and A. Winther, *Electromagnetic Excitation* (North-Holland, Amsterdam, 1975).
 - [22] M. Abramowitz and I. Stegun, *Handbook of Mathematical Functions* (Dover, New-York, 1970).
 - [23] Y. Sakuragi, M. Yahiro, and M. Kamimura, *Prog. Theor. Phys. Suppl.* **89**, 36 (1986).
 - [24] J. A. Tostevin, F. M. Nunes, and I. J. Thompson, *Phys. Rev. C* **63**, 024617 (2001).
 - [25] J. A. Tostevin *et al.*, *Phys. Rev. C* **66**, 024607 (2002).
 - [26] M. Takashina, S. Takagi, Y. Sakuragi, and Y. Iseri, *Phys. Rev. C* **67**, 037601 (2003).
 - [27] N. C. Summers and F. M. Nunes, *Phys. Rev. C* **70**, 011602(R) (2004).
 - [28] K. Ogata *et al.*, arxiv.org/nucl-th/0505007, 2005, submitted to *Phys. Rev. C*.
 - [29] F. M. Nunes, A. M. Mukhamedzhanov, C. C. Rosa, and B. Irgaziev, *Nucl. Phys. A* **736**, 255 (2004).
 - [30] F. M. Nunes and I. J. Thompson, *Phys. Rev. C* **57**, R2818 (1998).
 - [31] T. Kido, K. Yabana, and Y. Suzuki, *Phys. Rev. C* **50**, R1276 (1994).
 - [32] H. Esbensen, G. F. Bertsch, and C. A. Bertulani, *Nucl. Phys. A* **581**, 107 (1995).
 - [33] H. Esbensen and G. F. Bertsch, *Nucl. Phys. A* **600**, 37 (1996).
 - [34] V. S. Melezhik and D. Baye, *Phys. Rev. C* **59**, 3232 (1999).
 - [35] S. Typel and H. H. Wolter, *Z. Naturforsch. Teil A* **54**, 63 (1999).
 - [36] M. Fallot *et al.*, *Nucl. Phys. A* **700**, 70 (2002).
 - [37] P. Capel and D. Baye, *Phys. Rev. C* **71**, 044609 (2005).
 - [38] S. Typel and G. Baur, *Phys. Rev. C* **50**, 2104 (1994).
 - [39] S. Typel, H. H. Wolter, and G. Baur, *Nucl. Phys. A* **613**, 147 (1997).
 - [40] J. Mortimer, I. J. Thompson, and J. A. Tostevin, *Phys. Rev. C* **65**, 064619 (2002).
 - [41] F. Ajzenberg-Selove, *Nucl. Phys. A* **490**, 1 (1988).
 - [42] S. Typel and R. Shyam, *Phys. Rev. C* **64**, 024605 (2001).
 - [43] M. Zadro, *Phys. Rev. C* **70**, 044605 (2004).
 - [44] P. Capel, G. Goldstein, and D. Baye, *Phys. Rev. C* **70**, 064605 (2004).
 - [45] F. Ajzenberg-Selove, *Nucl. Phys. A* **506**, 1 (1990).
 - [46] P. Capel, G. Goldstein, and D. Baye, in *Proceedings of the Second Argonne/MSU/JINA/INT RIA Workshop on Reaction Mechanisms for Rare Isotope Beams*, edited by B. A. Brown (AIP, Melville, 2005), (In press).
 - [47] Z. Moroz *et al.*, *Nucl. Phys. A* **381**, 294 (1982).
 - [48] B. Bonin *et al.*, *Nucl. Phys. A* **445**, 381 (1985).
 - [49] F. D. Becchetti, Jr. and G. W. Greenlees, *Phys. Rev.* **182**, 1190 (1969).
 - [50] V. Guimarães *et al.*, *Phys. Rev. Lett.* **84**, 1862 (2000).
 - [51] J. J. Kolata *et al.*, *Phys. Rev. C* **63**, 024616 (2001).
 - [52] I. J. Thompson, *Comput. Phys. Rep.* **7**, 167 (1988).